

Multifunctional self-charging structures using piezoceramics and thin-film batteries

S R Anton, A Erturk and D J Inman

Center for Intelligent Material Systems and Structures, Department of Mechanical Engineering, Virginia Polytechnic Institute and State University, Blacksburg, VA 24061-0261, USA

E-mail: sranton@vt.edu

Received 26 May 2010, in final form 31 August 2010

Published 30 September 2010

Online at stacks.iop.org/SMS/19/115021

Abstract

Multifunctional material systems combine multiple functionalities in a single device in order to increase performance while limiting mass and volume. Conventional energy harvesting systems are designed to be added to a host structure in order to harvest ambient energy surrounding the system, but often cause undesirable mass loading effects and consume valuable space. Energy harvesting systems can benefit from the introduction of multifunctionality as a means of improving overall system efficiency. This paper presents the investigation of a novel multifunctional piezoelectric energy harvesting system consisting of energy generation, energy storage, and load bearing ability in a single device. The proposed self-charging structures contain piezoelectric layers for power generation, thin-film battery layers for energy storage, and a central metallic substrate layer, arranged in a bimorph configuration. Several aspects of the development and evaluation of the self-charging structure concept are reviewed. Details are provided on the fabrication of a piezoelectric self-charging structure. An electromechanical model is employed to predict the response of the harvester under harmonic base excitation. Experimentation is performed to confirm the ability of the device to simultaneously harvest and store electrical energy. Finally, both static and dynamic strength analyses are performed to determine the load bearing ability of the structure.

(Some figures in this article are in colour only in the electronic version)

1. Introduction

With recent growth in the development of low-power electronic devices such as microelectronics and wireless sensor nodes, the topic of energy harvesting has received much attention in the research community. Several modes of energy harvesting exist including conversion of solar, thermal, vibration, and wind energy to electrical energy. Among these schemes, piezoelectric vibration-based harvesting has been most heavily researched [1, 2]. Previous studies have investigated the modeling [3, 4], circuitry [5, 6], and various applications [7–9] of vibration energy harvesting using piezoelectric devices.

Traditional piezoelectric energy harvesting systems consist of an active harvesting element, conditioning circuitry, and a storage medium, where the sole function of the combined system is to convert ambient mechanical energy into usable electrical energy. Furthermore, conventional systems are designed as add-on components to a host structure, often

causing undesirable mass loading effects and consuming valuable space. A method of improving the functionality of conventional harvesting designs involves the use of a multifunctional approach in which the system not only harvests energy, but also performs additional tasks such as storing the scavenged energy or supporting mechanical load in the structure. In this work, the authors investigate a novel multifunctional approach to piezoelectric energy harvesting with the goal of creating a device capable of harvesting vibration energy, storing the harvested energy, and supporting structural loads.

Previous studies have investigated several different approaches to developing multifunctional structures. Christodoulou and Venables [10] give a review of some of the earlier efforts in multifunctional structures in which details are given on the development of structural power material systems, autonomous sensing and actuating material systems, electromagnetic multifunctional material systems, and sur-

vivable, damage-tolerant material systems. Of these four different classes of multifunctional material systems, structural power systems are of most interest for energy harvesting applications. Some of the original work on structural power systems, performed by Thomas and Qidwai [11–15], involves the development of multifunctional structures for unmanned vehicle applications. Thomas and Qidwai [11] first introduce the concept of the multifunctional *structure-battery* in which polymer–lithium-ion battery layers with structural additives are used to both store energy and support aerodynamic loads in an unmanned aerial vehicle (UAV) system. In a subsequent study, Thomas and Qidwai [12] provide formulations for the change in flight endurance of a UAV with an integrated structure-battery, and fabricate and perform flight testing on a small flying-wing UAV, called the WASP, which includes structure-batteries integrated into the wings. Additionally, the shear strength of several polymer–lithium-ion batteries is obtained experimentally as a means of quantifying the load bearing ability of the batteries.

More recently, Thomas and Qidwai have studied the use of structure-batteries in unmanned underwater vehicles (UUVs) [13–15]. Qidwai *et al* [13] describe the design and fabrication of structure-batteries specifically developed for marine systems, containing lithium-ion batteries embedded within fiber-reinforced polymer layers. Continuing the work, Rohatgi *et al* [14] present the experimental evaluation of the structure-batteries fabricated in [13]. The multifunctional composites are tested both mechanically via static three-point bend testing, and electrically through charge/discharge cycling of the battery layers. In their latest work, Qidwai *et al* [15] investigate the electrical performance of the various structure-battery designs while under load. Both static three-point bend testing and hydrostatic loading are considered while the charge/discharge performance of the composites is monitored.

Multifunctional solar energy harvesting systems have also been investigated in the literature and provide a means of combining structure and energy harvesting capabilities in a single device. Maung *et al* [16] introduce the ‘co-curing’ manufacturing process in which thin-film solar panels are directly integrated onto carbon-fiber-reinforced epoxy composites. Dennler *et al* [17] propose the concept of directly coupling a flexible solar panel with a conventional lithium–polymer battery to create a device that can both generate and store electrical energy. Several novel types of flexible solar panels are developed and considered for the device, and a unique interconnection layer is proposed for electrical connection of the solar panel and battery. Kim *et al* [18] expand upon the work of Dennler *et al* [17] and fabricate and test a solar power laminate consisting of thin-film solar panels and thin-film flexible lithium-based batteries connected with a flexible interconnect circuit.

Several studies have been performed in which various aspects of multifunctional structure power systems have been investigated. The next step in the development of these systems is to integrate structural function with energy storage and energy generation in a single multifunctional structure. Preliminary work by Dennler *et al* [17] and Kim *et al* [18] has examined solar energy harvesting multifunctional structures with integrated energy storage.

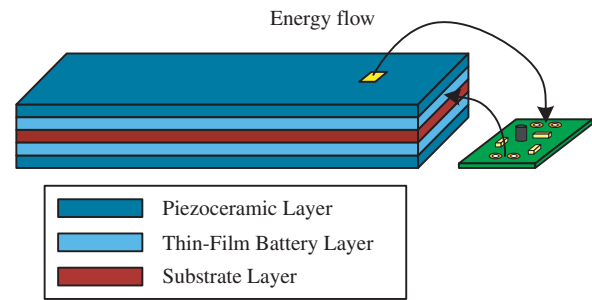


Figure 1. Schematic of self-charging structure.

It is the aim of this work to design, fabricate, and characterize a multifunctional piezoelectric vibration-based energy harvesting system with integrated energy storage and structural load bearing ability. Details of the design, material selection, and fabrication of the proposed multifunctional self-charging structures are given. An electromechanical assumed-modes formulation is employed to model multilayer, segmented piezoelectric energy harvester cantilever beams. The model is used to predict the coupled vibration and voltage response of the harvesters. Experimental testing is performed on the fabricated device in order to validate the electromechanical model and to prove the ability of the structures to simultaneously generate and store electrical energy. Lastly, the strength of the structures is investigated both statically through conventional three-point bending tests and dynamically by exciting the device at resonance under various excitation levels and monitoring for failures.

2. Self-charging structure concept

As previously stated, conventional piezoelectric energy harvesting systems are designed to be added to a host structure in order to harvest ambient energy, but often cause undesirable mass loading effects and consume valuable space. In order to improve the functionality and reduce the adverse loading effects of traditional piezoelectric harvesting approaches, the authors propose a multifunctional energy harvesting design in which a single device can generate and store electrical energy and also carry structural loads. The proposed self-charging structures, shown in figure 1, contain both power generation and energy storage capabilities in a multilayered, composite platform consisting of active piezoceramic layers for scavenging energy, thin-film battery layers for storing scavenged energy, and a central metallic substrate layer arranged in a bimorph configuration. The operational principle behind the device involves simultaneous generation of electrical energy when subjected to dynamic loading causing deformations in the structure, as well as energy storage in the thin-film battery layers. Energy is transferred directly from the piezoceramic layers through appropriate conditioning circuitry to the thin-film battery layers, thus a single device is capable of both generating and storing electrical energy. Additionally, the self-charging structures are capable of carrying loads as structural members due to the stiffness of the composite device.

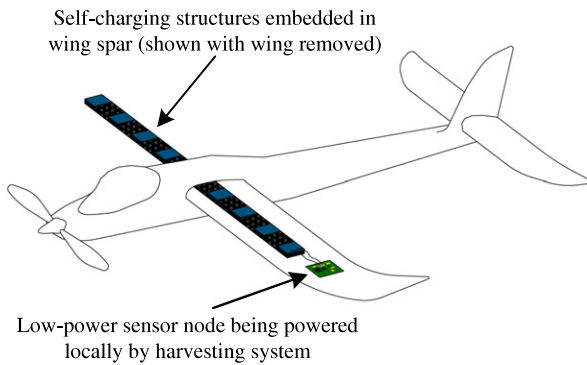


Figure 2. Potential use of self-charging structures: schematic of small UAV with embedded self-charging structures in wing spar used to provide local power for low-power sensor node.

The ability of the device to harvest energy, store energy, and support structural loads provides true multifunctionality.

The fruition of the self-charging structure concept is mainly attributed to the development of novel thin-film battery technology which allows for the creation of thin, lightweight, and flexible batteries. Conventional energy storage devices, such as capacitors and traditional rechargeable batteries, are large, bulky devices which add significantly to the overall mass and volume of the harvesting system. Additionally, traditional storage devices are not suitable for direct integration into the active element of an energy harvesting system as their mass, volume, and rigidity would hinder the ability of the device to harvest energy. Mechanical failure is also a concern with conventional storage elements as they may fail under the loads applied to the harvester. Thin-film lithium-based batteries provide a viable solution for self-charging structures. The batteries are flexible and have a typical thickness on the order of less than a millimeter, mass of around 0.5 g, and capacity in the milliamp-hour range. The small capacities of these batteries are a good match for the low electrical output levels associated with piezoelectric energy harvesting, and their thin, lightweight platform is ideal for direct integration into piezoelectric harvesters to create compact, multifunctional self-charging structures.

A novel aspect of the self-charging structure concept is that the composite harvester can be used as a load bearing member in a host structure. The harvester can be embedded into or used in place of an existing component, thus reducing the total mass added to the host structure. A potential application that can benefit from the energy harvesting, energy storage, and load bearing capabilities of self-charging structures, for example, is in powering remote, low-power sensors in UAVs. Such multifunctional composite harvesting devices can be embedded into the wing spar of a UAV, as shown in figure 2, with the goal of providing a local power source for remote low-power wireless sensors such as accelerometers, structural health monitoring nodes, or even low-power imaging devices or cameras. Providing a local power source composed of both harvesting and storage elements is beneficial because it eliminates the need to run wires and tap into the propulsive power supply of the aircraft, thus reducing mass and complexity while allowing the sensors

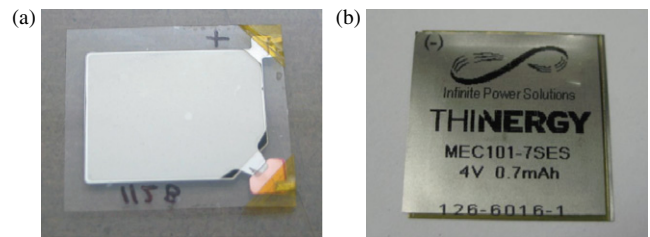


Figure 3. Photographs of (a) NanoEnergy® and (b) Thinerger® thin-film batteries.

to operate wirelessly. Additionally, a multifunctional approach in which the composite harvester is embedded into the wing spar and supports structural loads in the wings is valuable because it can reduce or eliminate the added mass of the harvesting device.

While the wing spar example above presents one potential use of self-charging structures, the technology can be used in any low-power application that can benefit from a multifunctional harvesting solution. Embedded electronic systems and remote self-powered sensor nodes are examples of applications where the added mass and volume of conventional harvesting could present design challenges, and where the multifunctional approach of self-charging structures can be beneficial. Additionally, when coupled with an appropriate piezoelectric device, the mechanical properties of the self-charging structure can be tailored to meet the needs of various applications. Piezoelectric devices range from stiff, brittle monolithic piezoceramic to flexible piezoelectric fiber-based transducers, allowing a wide range of mechanical properties to be obtained, thus making the self-charging structure a versatile energy harvesting solution.

3. Evaluation of thin-film batteries

NanoEnergy® thin-film batteries manufactured by Front Edge Technology, Inc. (Baldwin Park, CA) and Thinerger® thin-film batteries produced by Infinite Power Solutions, Inc. (Littleton, CO) are both investigated in this research. Both batteries, shown in figure 3, are flexible lithium-based secondary (i.e. rechargeable) cells that utilize all solid-state components. Common to both types of thin-film batteries, the active elements include lithium metal anodes, lithium cobalt dioxide (LiCoO_2) cathodes, and lithium phosphorous oxynitride (LiPON) electrolyte layers. The ability to produce extremely thin (less than $200 \mu\text{m}$) and flexible batteries can be attributed to the use of the solid-state LiPON electrolyte as opposed to liquid or gel electrolytes found in conventional rechargeable batteries. LiPON, developed at Oak Ridge National Laboratory [19, 20], exhibits a high lithium-ion mobility, lending to its performance as an electrolyte, and a low electron mobility, allowing for low self-discharge rates.

3.1. Comparison to conventional rechargeable batteries

Compared to traditional rechargeable batteries, thin-film batteries offer a clear advantage in form factor. Table 1

Table 1. Properties of various secondary batteries.

Battery	Voltage (V)	Capacity (mAh)	Mass (g)	Volume (cm ³)	Specific energy (Wh kg ⁻¹)	Energy density (Wh l ⁻¹)
Energizer NH15-2450 NiMH AA	1.2	2450	30.00	8.34	98.00	352.52
Energizer NH22-175 NiMH 9V	8.4	175	42.00	21.52	35.00	68.31
Varta V15H NiMH button type	1.2	15	1.30	0.32	13.85	60.00
Samsung AB463446FZ Li-ion cell phone	3.7	800	17.90	8.36	165.36	354.07
AA Portable Power Corp. PL-383562-C2 Li-Polymer Single Cell	3.7	850	18.00	7.26	174.72	433.26
Front Edge Technology, Inc. NanoEnergy [®] Lithium thin-film	4.2	4	0.45	0.11	76.36	152.73
Infinite Power Solutions, Inc. Thinergy [®] MEC101-7 Lithium thin-film	4.0	0.7	0.22	0.11	6.22	25.45

presents both physical and electrical properties of various types of secondary batteries, in which the mass and volume of both NanoEnergy[®] and Thinergy[®] batteries are shown to be 1–2 orders of magnitude less than those of conventional rechargeable batteries. Thin-film batteries are also flexible, where conventional batteries are rigid, and thin-film battery technology offers superior cycle life (on the order of 1000–10 000 cycles) compared to conventional rechargeable designs (typically 100–1000 cycles). The main drawback to thin-film battery technology lies in the low storage capacity of the cells, which in turn causes the energy density and specific energy of the batteries to suffer (see table 1). The Thinergy[®] cells exhibit a much lower energy density and specific energy than the NanoEnergy[®] cells, mainly due to the increased amount of packaging material used. Although their small capacity restricts their use to low energy applications, the flexibility, slimness, and superior cycle life of thin-film batteries allows them to be used in applications where previously impractical, such as direct integration into composite structures, thus creating countless new possibilities for energy storage systems.

Another important difference between conventional batteries and thin-film lithium-based batteries is the internal resistance of the cells. The thin-film batteries investigated in this study have typical internal resistances on the order of 50–200 Ω . This is extremely high compared to the internal resistances of most conventional alkaline, nickel–metal hydride, and lithium-ion secondary batteries which are on the order of 0.1–1 Ω . As current flows through a battery, there is a voltage drop across the internal resistance (indeed proportional to the internal resistance) of the battery, thus a large internal resistance is detrimental to battery performance.

3.2. Battery selection

Both NanoEnergy[®] and Thinergy[®] cells are considered for use in self-charging structures. The primary difference between the cells lies in the packaging material and encapsulation method. NanoEnergy[®] thin-film batteries are built by encasing

the active elements between a top and bottom mica substrate and sealing the substrate layers with a Surlyn[®] (DuPont, Wilmington, Delaware) sealant layer around the perimeter of the active elements. Electrical leads are given in the form of 100 μm thick metal foil tabs. Thinergy[®] batteries are assembled using a proprietary encapsulation method, however, it can be observed that they utilize a metal foil substrate for the top and bottom outer layers, which act as electrodes, and a sealant layer between the electrode layers to prevent electrical shorting. Preliminary testing of both types of thin-film batteries has revealed that the metal foil substrate of the Thinergy[®] batteries facilitates convenient electrode application as opposed to the metal foil tabs of the NanoEnergy[®] cells, which are fragile and difficult to use. Additionally, the metal foil substrate also appears more robust compared to the mica substrate used on the NanoEnergy[®] cells, which can peel away from the sealant under shear loading. Previous research has reported similar observations in regards to the fragility of the NanoEnergy[®] cells [21, 22]. Although the capacity of the NanoEnergy[®] batteries is superior to that of the Thinergy[®] cells (see table 1), Thinergy[®] batteries are selected for use in self-charging structures due to their increased robustness.

The Thinergy[®] batteries used in this study have a nominal operating voltage of 4.0 V and a nominal capacity of 0.7 mAh. Typical dimensions are 25.40 mm \times 25.40 mm with a thickness of 170 μm and a mass of about 0.450 g. Infinite Power Solutions claims that the Thinergy[®] cells can exhibit 10 000 cycles at 100% depth of charge before deteriorating to 80% of the initial capacity at a C/2 discharge rate. They also state that the batteries can be charged to 90% of rated capacity in 10 min and can be discharged at rates up to 40C.¹ (Note that battery charge and discharge currents are given in terms of their rated capacity, C. A rate of 40C for a battery with a capacity of 0.7 mAh corresponds to a current of 28 mA.)

¹ www.infinitepowersolutions.com.

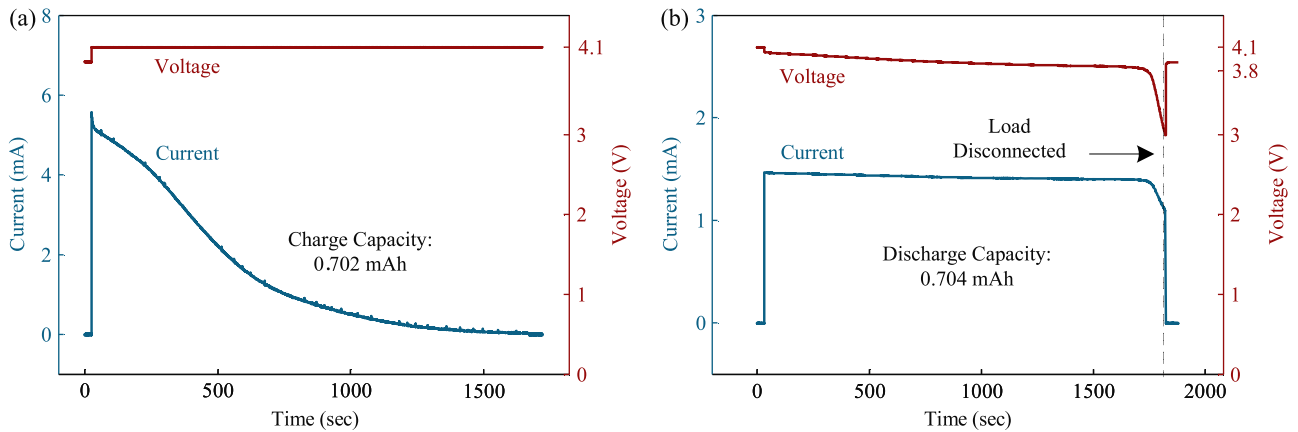


Figure 4. Characteristic (a) charge and (b) discharge curves of the Thinerger[®] batteries.

3.3. Performance testing of Thinerger[®] batteries

Prior to combining the Thinerger[®] thin-film batteries with piezoelectric devices to create self-charging structures, the performance of the batteries is evaluated experimentally. The batteries are charged using an HP 6825A power supply/amplifier, which provides constant-voltage charging, and discharged through standard carbon film resistors. During charging and discharging, the battery voltage as well as the current flowing in/out of the battery are monitored and recorded using a National Instruments CompactDAQ chassis and a NI 9215 four-channel analog voltage input card. In order to measure the current flowing through the battery, a transimpedance operational amplifier circuit is used to convert the current into a voltage that is measurable with the NI 9215 card. The capacity achieved during charging and discharging can be calculated by performing numerical integration of the current measurement over time as follows [21, 22]:

$$C = \int i dt. \quad (1)$$

Typical voltage and current measurements during charging and discharging of the Thinerger[®] batteries are shown in figures 4(a) and (b), respectively. Charging is performed by supplying 4.1 V of potential to the battery using the power supply until only about 35 μ A of current is sourced by the battery, at which time the battery is considered fully charged. Discharging is performed by applying a resistive load of 2749 Ω across the battery in order to draw 2C (1.4 mA) until a voltage of 3.0 V (the cutoff voltage recommended by the manufacturer) is reached. A rate of 2C is chosen arbitrarily in order to provide a reasonable time to discharge the battery (approximately 30 min). The batteries are capable of discharge rates up to 40C, however, such large discharge rates can degrade the performance of the batteries over time. The charge and discharge characteristics displayed are typical for rechargeable batteries. For this particular battery, an initial voltage drop during discharging of 0.061 V (from 4.096 to 4.035 V) and a current of 1.467 mA are observed. The corresponding internal resistance of this battery can be calculated using the relation $R_{\text{int}} = V_{\text{drop}}/I$ as 41.58 Ω , which

is slightly below the manufacturer's specification of 50 Ω . Carrying out the capacity calculation given in equation (1), the capacity in charging is calculated as 0.702 mAh, and in discharging as 0.704 mAh, which correlate well with the manufacturer's specification of 0.7 mAh. It is expected that these capacities be reasonably close to one another, which is the case, and in both charging and discharging, the full 0.7 mAh capacity can be obtained. Overall, the Thinerger[®] battery performs as expected, showing reasonable charge/discharge characteristics and good charge cycling ability.

4. Fabrication details of self-charging structures

Assembly of the self-charging structures involves several steps including the selection of piezoelectric and substrate materials, bonding the battery, piezoelectric, and substrate layers, and connecting leads to the electrodes of the thin-film batteries and piezoelectric devices. These steps are outlined in the following sections.

4.1. Selection of piezoelectric and substrate materials

A commercially available piezoelectric material will be used as the active energy harvesting element in this research. Several types of piezoelectric material exist, from polymer films with low elastic moduli and electromechanical coupling, to piezoelectric fiber-based devices with increased stiffness and moderate coupling, to brittle monolithic ceramics with high electromechanical coupling. As a compromise between the high energy generation of monolithic ceramics and the strength and flexibility of fiber-based devices, QuickPack[®] piezoelectric devices (Midé Technology Corp., Medford, MA) are selected for use in self-charging structures. QuickPack[®] devices contain monolithic piezoceramic (PZT-5A) active elements bracketed by kapton layers to protect the active element and provide additional robustness.

Several substrate materials can be considered for use in self-charging structures. Typical piezoelectric bimorph energy harvesters contain a thin, relatively flexible substrate, such as brass or aluminum, such that the stiffness of the substrate does

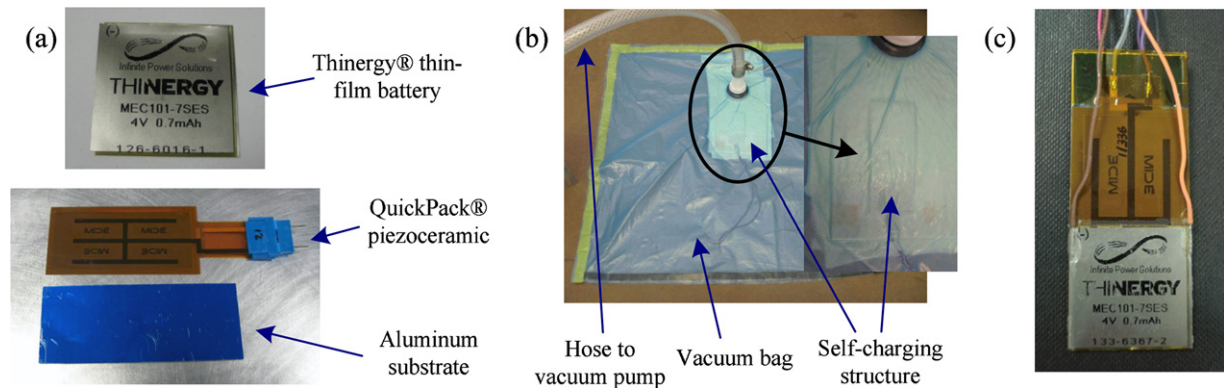


Figure 5. (a) Components used in self-charging structure; (b) vacuum bagging setup; (c) complete self-charging structure.

Table 2. Physical parameters of self-charging structure components.

Parameter	Aluminum substrate	QP10N device	QP10N active element	Thinergy® batteries
Thickness (mm)	0.127	0.381	0.254	0.178
Width (mm)	25.400	25.400	20.574	25.400
Length (mm)	63.500	50.800	45.974	25.400
Mass (g)	0.530	2.250		0.460

not dominate the overall structural stiffness in order to allow adequate vibration energy to be induced in the piezoelectric elements. The substrate layer material selected in this study for use in the self-charging structures is 1100-O aluminum alloy. Alternative substrates can be used, however, to alter the characteristics of the self-charging structures to fit the design parameters of a given application.

Important physical parameters of the various components used to construct the prototype self-charging structure, shown in figure 5(a), are given in table 2. As stated previously, the QuickPack® devices consist of a central monolithic piezoceramic (PZT-5A) layer bracketed by 0.0635 mm thick kapton layers that include embedded electrodes. Dimensions of both the overall device and the active element are given in the table.

4.2. Vacuum bonding and electrode attachment

Fabrication of the self-charging structures is performed by separately bonding each layer using a vacuum bagging procedure, shown in figure 5(b), to achieve thin, uniform bonding layers. 3M ScotchWeld™ DP460 two-part epoxy is chosen for the bonding layer due to its high shear strength (27.58 MPa when bonded to aluminum) and high volume resistivity (2.4×10^{14} ohm cm). Bonding is achieved by applying a thin layer of epoxy between two component layers, placing the device in vacuum, and allowing it to cure for 6 h. The thin-film batteries are selected as the outermost layers to facilitate attachment of electrical leads. They are placed towards the free end of the device to reduce the induced strain in the batteries in order to help prevent electrical or mechanical failure.

With all of the self-charging structure layers bonded, the final step in fabrication involves attaching electrical leads to both the piezoceramic and battery layers. 22-gauge insulated and stranded wire is soldered to both the QuickPack® layers and battery layers to provide electrical connections. Care is taken when soldering leads to the Thinergy® batteries to prevent shorting as connection to the bottom electrode is given via a thin overlapping strip accessible from the top surface. Additionally, an epoxy coating is placed over the electrical connections on the battery to provide electrical isolation and increased mechanical strength. A photograph of a complete self-charging structure with electrical leads can be seen in figure 5(c).

5. Electromechanical modeling

The most common form of a vibration-based energy harvesting device is the cantilever beam attached to a vibrating host structure and subject to base excitation. In this work, the self-charging structures are modeled and tested in the cantilever configuration to evaluate their energy harvesting capability. Distributed-parameter analytical solutions for cantilevered unimorph [3], bimorph [23], and multimorph [24] energy harvester beams have been presented in the recent literature. Convergence of the electromechanical Rayleigh–Ritz formulation [25, 4] to the analytical solution [3] for sufficient number of kinematically admissible functions has been reported in the literature [4]. Assumed-modes formulation [26] is an alternative way of describing the spatially discretized system dynamics and the resulting equations are identical to those of the Rayleigh–Ritz method. Both of these techniques are preferred especially for structures with varying geometric or material properties such as multi-segment structures. The two-segment self-charging structures developed in this work are modeled using the assumed-modes technique. The following is a summary of the derivation.

The cantilevered self-charging structure shown in figure 6 consists of two uniform regions in the longitudinal direction (x -direction). The region $0 \leq x \leq L_1$ has piezoceramic, substructure, kapton as well as high shear strength epoxy layers used for bonding while the region $L_1 \leq x \leq L$ has two thin-film battery layers and two more epoxy layers in

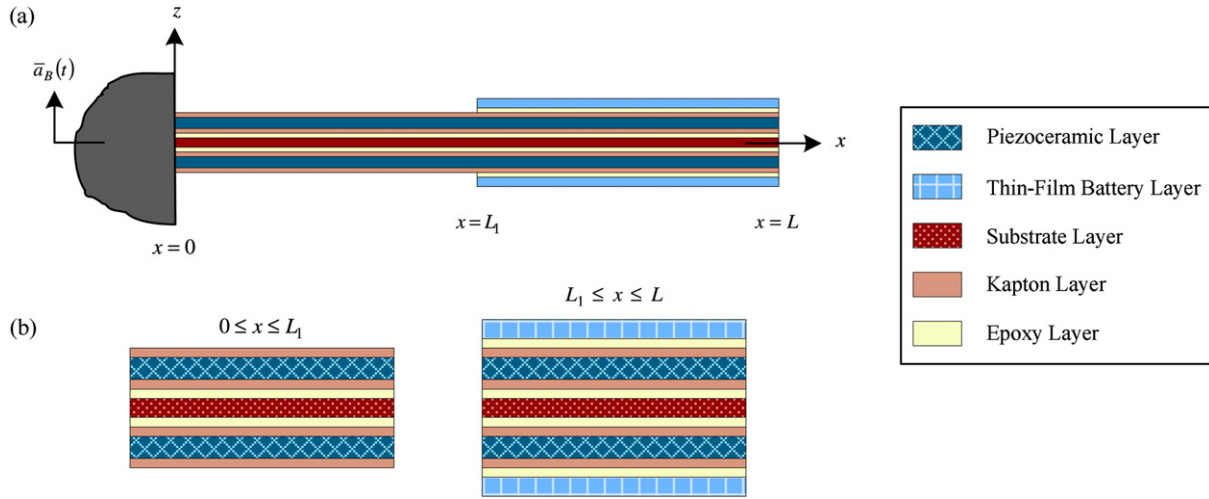


Figure 6. (a) Schematic of self-charging structure with piezoceramic, battery, substrate, kapton, and epoxy layers; (b) cross-sectional views of the two regions.

addition to the layers of the former region. The structure is excited under translational base acceleration imposed in the transverse direction (z -direction) at the clamped end. The cantilevered structure is assumed to be sufficiently thin so that the shear deformation and rotary inertia effects are negligible for the practical modes of interest (the fundamental mode is of particular interest in energy harvesting), hence the derivation is based on the Euler–Bernoulli beam assumptions. The reader is referred to [26] for Rayleigh and Timoshenko type energy harvester models to describe the dynamics of moderately thick energy harvester beams. The electrode pairs (of negligible thickness) covering the opposite faces of each piezoceramic layer are assumed to be perfectly conductive so that a single electric potential difference can be defined across them.

The extended Hamilton's principle with internal electrical energy is [26]

$$\int_{t_1}^{t_2} (\delta T - \delta U + \delta W_{ie} + \delta W_{nc}) dt = 0 \quad (2)$$

where δT , δU , and δW_{ie} are the first variations of the total kinetic energy (T), the total potential energy (U) and the internal electrical energy (W_{ie}), and δW_{nc} is the virtual work of the non-conservative mechanical force and electric charge components. The effect of base excitation is considered in the total kinetic energy term and proportional mechanical damping effect is to be introduced in the spatially discretized form, therefore the only non-conservative virtual work is due to the electric charge output (Q):

$$\delta W_{nc} = \delta W_{nce} = Q\delta v \quad (3)$$

where v is the voltage across the external load.

The vibration response of the beam relative to its moving base is

$$w(x, t) = \sum_{i=1}^N \phi_i(x) \eta_i(t) = \Phi^T(x) \eta(t) \quad (4)$$

where $\Phi(x)$ is the vector of admissible functions, $\eta(t)$ is the vector of generalized modal mechanical coordinates, N is the total number of mechanical modes used in the expansion and the superscript T stands for transpose. A simple admissible function that satisfies the essential boundary conditions of a clamped-free thin beam is [27, 4]

$$\phi_i(x) = 1 - \cos\left(\frac{(2i-1)\pi x}{2L}\right) \quad (5)$$

where i is the modal index.

The electromechanical Lagrange equations are given for the generalized coordinates η_i and v as [26]

$$\frac{d}{dt} \left(\frac{\partial T}{\partial \dot{\eta}_i} \right) - \frac{\partial T}{\partial \eta_i} + \frac{\partial U}{\partial \eta_i} - \frac{\partial W_{ie}}{\partial \eta_i} = 0 \quad (6)$$

$$\frac{d}{dt} \left(\frac{\partial T}{\partial \dot{v}} \right) - \frac{\partial T}{\partial v} + \frac{\partial U}{\partial v} - \frac{\partial W_{ie}}{\partial v} = Q \quad (7)$$

which yield the governing equations

$$\mathbf{M}\ddot{\eta}(t) + \mathbf{C}\dot{\eta}(t) + \mathbf{K}\eta(t) - \Theta v(t) = -\mathbf{F}a_B(t) \quad (8)$$

$$C_p^{\text{eq}} \dot{v}(t) + \frac{v(t)}{R_1} + \Theta^T \dot{\eta}(t) = 0 \quad (9)$$

where \mathbf{M} , \mathbf{C} , and \mathbf{K} are the mass, damping, and stiffness matrices, \mathbf{F} is the effective forcing vector, Θ is the electromechanical coupling vector, C_p^{eq} is the equivalent capacitance, R_1 is the external load resistance and an over-dot represents differentiation with respect to time. In equations (8) and (9), proportional damping is assumed so that standard modal analysis can be used with mathematical convenience (i.e. the damping matrix has the form $\mathbf{C} = \alpha\mathbf{M} + \beta\mathbf{K}$ where α and β are constants of proportionality).

If the base acceleration is assumed to be harmonic of the form $a_B(t) = \bar{a}_B e^{j\omega t}$ (where ω is the excitation frequency and j is the unit imaginary number), the steady-state voltage

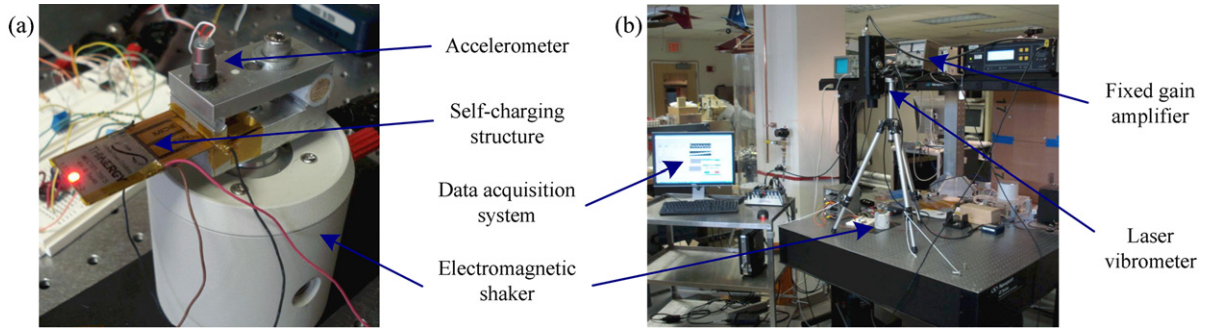


Figure 7. (a) Self-charging structure mounted to shaker and (b) overall experimental setup for vibration testing.

response and vibration response can be obtained as

$$v(t) = j\omega \left(\frac{1}{R_l} + j\omega C_p \right)^{-1} \Theta^T \left(\mathbf{K} - \omega^2 \mathbf{M} + j\omega \mathbf{C} + j\omega \left(\frac{1}{R_l} + j\omega C_p \right)^{-1} \Theta \Theta^T \right)^{-1} \mathbf{F} \bar{a}_B e^{j\omega t} \quad (10)$$

$$w(x, t) = -\Phi^T(x) \left(\mathbf{K} - \omega^2 \mathbf{M} + j\omega \mathbf{C} + j\omega \left(\frac{1}{R_l} + j\omega C_p \right)^{-1} \Theta \Theta^T \right)^{-1} \mathbf{F} \bar{a}_B e^{j\omega t}. \quad (11)$$

The voltage output-to-base acceleration and the vibration response-to-base acceleration frequency response functions (FRFs) can be extracted as $v(t)/\bar{a}_B e^{j\omega t}$ and $w(x, t)/\bar{a}_B e^{j\omega t}$, respectively. Note that, in this approximate analytical solution technique, sufficient number of admissible functions should be used for convergence of the natural frequencies of interest to the exact values [4, 26].

6. Experimental validation of self-charging structure concept

Experiments are performed on the fabricated self-charging structure shown in figure 5(c) in order to confirm the ability of the device to simultaneously harvest and store electrical energy. The performance of the self-charging structure is evaluated by mounting the device in a cantilever fashion and subjecting it to base excitations while monitoring the energy transfer between the piezoceramic layers and the battery layers. The following sections describe the results of the experimental characterization.

6.1. Frequency response measurements

The self-charging structure is clamped to a small TMC Solution Dynamic TJ-2 electromagnetic shaker with an overhang length of 43.7 mm, as shown in figure 7(a). In order to determine the resonant frequency and optimal load resistance of the clamped device, experiments are conducted to obtain the electromechanical FRFs of the self-charging structure for a set of resistive electrical loads (ranging from 100 Ω to 1 M Ω). SigLab data acquisition hardware is used for all FRF measurements. The input acceleration is measured using a PCB U352C67 accelerometer, the tip velocity is

measured using a Polytec OFV303 laser Doppler vibrometer, and the voltage output of the self-charging structure is measured directly with the SigLab data acquisition system. The overall test setup is shown in figure 7(b).

For the series connection of the piezoceramic layers (to obtain larger voltage output), the voltage output-to-base acceleration and tip velocity response-to-base acceleration FRFs of the self-charging structure are shown in figures 8(a) and (b), respectively (where the base acceleration is given in terms of the gravitational acceleration, $g = 9.81 \text{ m s}^{-2}$). To verify the electromechanical model developed for the prediction of the output of the harvester, the voltage output and the vibration response FRFs are predicted using equations (10) and (11), respectively, and plotted over the experimental results in figure 8. Twenty modes are used in the assumed-modes formulation ($N = 20$) to ensure the convergence of the fundamental natural frequency using the admissible functions given by equation (5). As the load resistance is increased from 100 Ω to 1 M Ω , the experimental value of the fundamental resonance frequency moves from 204.0 Hz (close to short-circuit conditions) to 211.1 Hz (close to open-circuit conditions). These two frequencies are the short-circuit and the open-circuit resonance frequencies and they are predicted by the electromechanical model as 204.1 Hz and 211.0 Hz, respectively. The amplitude-wise model predictions are also in agreement with the experimental measurements. It is worth mentioning that the maximum voltage output is obtained for the largest load resistance for excitation at the open-circuit resonance frequency as 34 V g^{-1} (peak amplitude). The optimal electrical loads for excitations at 204.0 Hz and 211.1 Hz are identified as 9.8 k Ω and 91.0 k Ω (among the resistors used), respectively, which yield similar experimental peak power outputs of 2.8 mW g^{-2} and 3.1 mW g^{-2} , respectively. These voltage and power output values given in terms of base acceleration are, however, frequency response-based linear estimates obtained from low-amplitude chirp excitation and they are not necessarily accurate for large-amplitude excitations with nonlinear response characteristics.

After the preliminary analysis for the resistive load case, the piezoceramic and thin-film battery layers are connected to the input and output of a simple linear voltage regulator circuit (consisting of a full bridge rectifier, smoothing capacitor, and voltage regulator), respectively. The electrical boundary conditions of the piezoceramic layers then become more

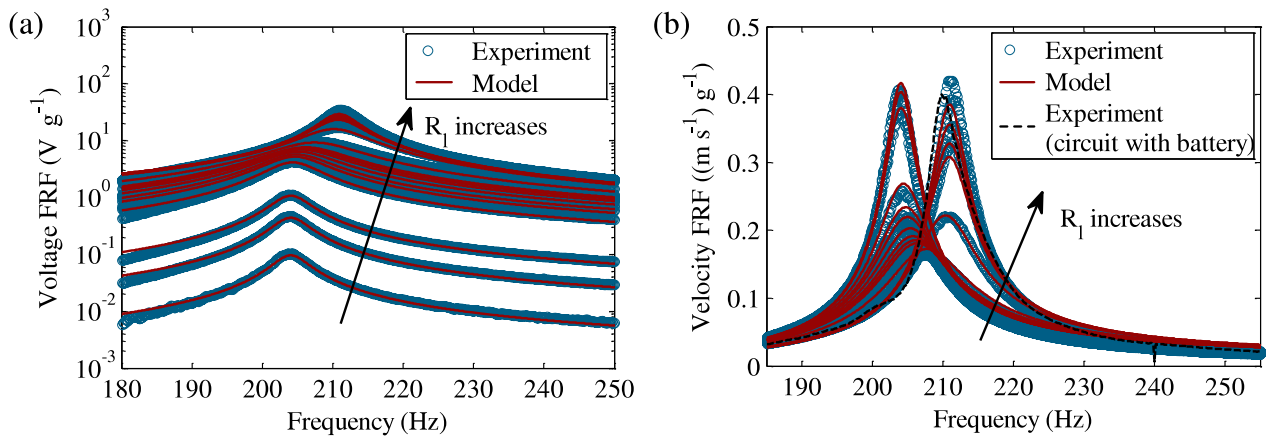


Figure 8. The (a) voltage-to-base acceleration and (b) tip velocity-to-base acceleration FRFs of the self-charging structure for a set of resistive loads.

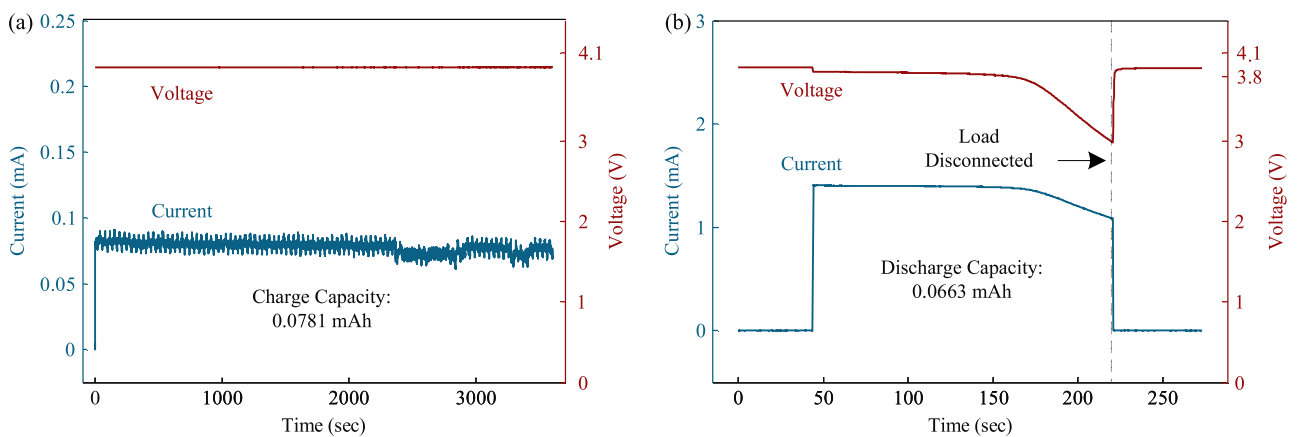


Figure 9. Experimental curves for self-charging structures in (a) charging and (b) discharging under $\pm 1.0 g$ acceleration at 210.0 Hz.

sophisticated. The tip velocity FRF is measured for this case, and is plotted in figure 8(b). It appears from the figure that the case with the largest resistive load ($1 M\Omega$, close to open-circuit conditions) successfully represents the vibration response of the self-charging structure when connected to the circuit, which exhibits resonance around 210.0 Hz.

6.2. Electrical charge/discharge measurements

With the resonant frequency of the self-charging structure connected to the circuit obtained, the energy harvesting performance of the device can be experimentally evaluated. Using the same experimental setup shown in figure 7, the self-charging structure is excited at resonance (210.0 Hz) with the piezoelectric layers configured to charge the thin-film battery layers through the linear voltage regulator circuit. For this experimentation, the two piezoelectric layers are connected in series for increased voltage output and used to charge a single battery layer. The input base acceleration amplitude is set to $\pm 1.0 g$. The device is excited for 1 h and the battery voltage and current into the battery are measured throughout the test. Once the test is complete, the battery is discharged using a 2749Ω resistor in order to draw 2C of current out of the battery. Results from both the charging and discharging tests

are shown in figure 9. From figure 9(a), it can be seen that the piezoelectric layers are able to supply an average of about 0.08 mA of current into the battery. Using equation (1), the capacity during charging is found to be 0.0781 mAh. During discharging, the current output is held at 1.4 mA for about 120 s before beginning to decay and a capacity of 0.0663 mAh is found by integrating the current over time. There is a slight difference between the capacities calculated in charging and discharging, which is likely a leakage effect where some of the energy during charging is dissipated in the battery, thus there is a small decrease in capacity when discharging.

The charge/discharge results presented in figure 9 prove the ability of the self-charging structures to simultaneously generate and store electrical energy in a multifunctional manner, and validate the concept of self-charging. Furthermore, the current of 0.08 mA corresponds to an average power of around 0.306 mW during charging. This is a reasonable value for piezoelectric energy harvesting, where typical harvested powers are in the microwatt to milliwatt range [1].

7. Strength analysis

It has been proposed that the self-charging structures developed in this work be directly integrated into host structures in

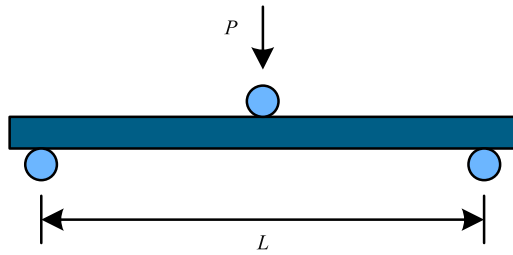


Figure 10. Schematic of three-point bending test fixture.

a multifunctional manner. Inherent in this proposal is the fact that the self-charging structures must act as load bearing members. Both static and dynamic testing is carried out in order to determine the strength of the self-charging structures. Results of the strength testing can be used as a design tool in the development of embedded self-charging structure systems. The following sections outline the formulations and procedures used to define the failure strength of the self-charging structures, as well as the results of experimental failure testing.

7.1. Static failure analysis and testing

Bending tests (or flexure tests) are usually employed to evaluate tensile strengths of brittle materials [28] (such as the piezoceramic layers in the case of self-charging structures). Classical three-point bending tests are performed in this study in order to experimentally evaluate the strength of the various components of the self-charging structures as well as the complete assembly. A schematic of a three-point bending test setup is shown in figure 10. The transverse load, P , is applied at the center ($x = L/2$) of the uniform rectangular beam with support span L , therefore, the maximum bending moment occurs at this point ($M_{\max} = PL/4$). The static load, P_f , required for transition from elastic material behavior to either plastic behavior (for ductile materials) or abrupt failure (for brittle materials) is considered in this work as the mechanical failure load that leads to the mechanical failure strength. The maximum bending moment that corresponds to the failure load (P_f) of the assembly is defined as the failure bending moment (M_f).

The bending strength of a simple beam placed under three-point bending is defined from Euler–Bernoulli beam theory as

$$\sigma_b = \frac{3L}{2bh^2} P_f \quad (12)$$

where b is the sample width, and h is the sample thickness.

The maximum bending stress of a given layer of a multilayer composite device, such as the complete self-charging structure assembly, can be defined as

$$\sigma_b^{\max} = \frac{Y_k h_{kn}}{\bar{YI}} M_f = \frac{Y_k h_{kn} L}{4\bar{YI}} P_f \quad (13)$$

where σ_b^{\max} is the maximum stress of a layer at a given failure load of the device, Y_k is the elastic modulus of the layer of interest (layer k), h_{kn} is the distance from the neutral axis to

the outer surface of the k th layer, and \bar{YI} is the overall bending stiffness of the multilayer beam. In order to obtain the value of \bar{YI} of a multilayer beam, a cross-section transformation (as described by Erturk and Inman [3]) can be used. In addition, a beam-like aspect ratio is assumed in the foregoing derivation and thin-plate parameters can be used for bending of plate-like configurations [26].

Equation (12) gives the failure strengths of the individual layers under separate loading, whereas equation (13) can be used to estimate the maximum stresses of the individual layers for the failure load of the assembly. It is worth mentioning that the maximum stress of a layer for the failure load of the assembly might be lower than its individual failure strength. For instance, for the failure load that results in fracture of a piezoceramic layer in a multilayer assembly, the maximum stress in the metallic layer could be lower than its individual failure strength. Nevertheless, the overall structure is assumed to be failed when any layer starts exhibiting brittle or ductile failure behavior.

Experimental testing is performed using an Instron 4204 universal test frame equipped with a 1000 N load cell and a small three-point bend fixture with adjustable supports, shown in figure 11(a). Each specimen rests on the two lower support pins, which are spaced 20 mm apart, and the central pin is lowered using the machine at a rate of 0.3 mm min^{-1} until a prescribed displacement is reached. In each case, the specimens fail before the maximum displacement is achieved.

Three individual samples are tested for the aluminum substrate, QP10N piezoceramic, and Thinerger[®] battery layers. Conventionally, three-point bend testing is performed on beam-shaped samples in order to eliminate Poisson effects. It is desirable, however, to test the Thinerger[®] battery samples in an unmodified state as dicing the batteries could result in damage to the packaging and delamination, therefore, plate-like samples are tested in this work. Additionally, the QuickPack[®] samples are not uniform across their cross-section due to the embedded electrodes in the kapton layers, thus cutting beam-shaped samples out of the device would give samples of varying composition. The Thinerger[®] samples are tested without modification, the aluminum specimens are cut to $25.4 \text{ mm} \times 25.4 \text{ mm}$, and the QuickPack[®] samples are cut in half (resulting in two identical samples of about $25.4 \text{ mm} \times 25.4 \text{ mm}$) to fit in the test fixture. A single self-charging structure is tested and cut in half such that each section can be tested separately. Photographs of the two self-charging sections after failure testing are shown in figures 11(b) and (c). The load and crosshead displacement are recorded throughout each test, and typical load–deflection curves for the individual layers as well as the complete structure are shown in figure 12. From the results presented in figure 12(a), it is clear that the individual QuickPack[®] piezoceramic layers exhibit brittle failure and the individual aluminum substrate and Thinerger[®] battery layers exhibit ductile failure. In the case of the aluminum sample, the failure load is taken where a slight, prolonged drop in the force is observed, as noted in the figure. From figure 12(b), it can be seen that the root section of the self-charging structure experiences brittle failure, where the tip section exhibits simultaneous ductile and brittle failure

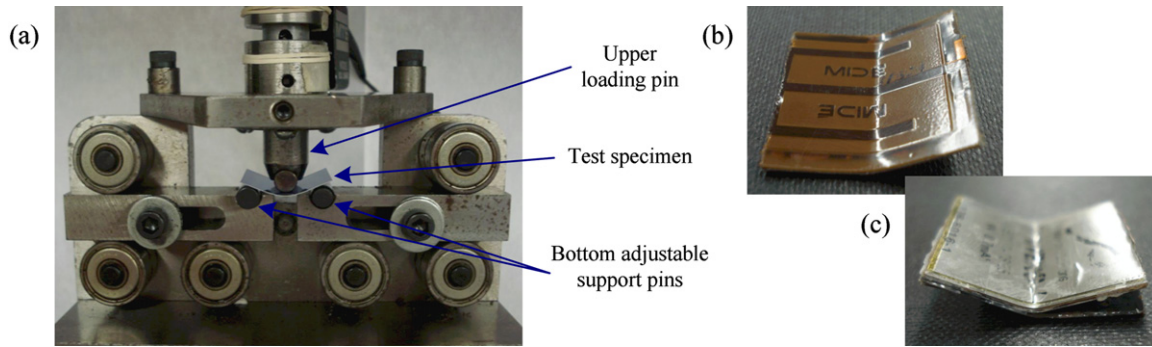


Figure 11. (a) Three-point bend fixture; self-charging structures after failure (b) root section, (c) tip section.

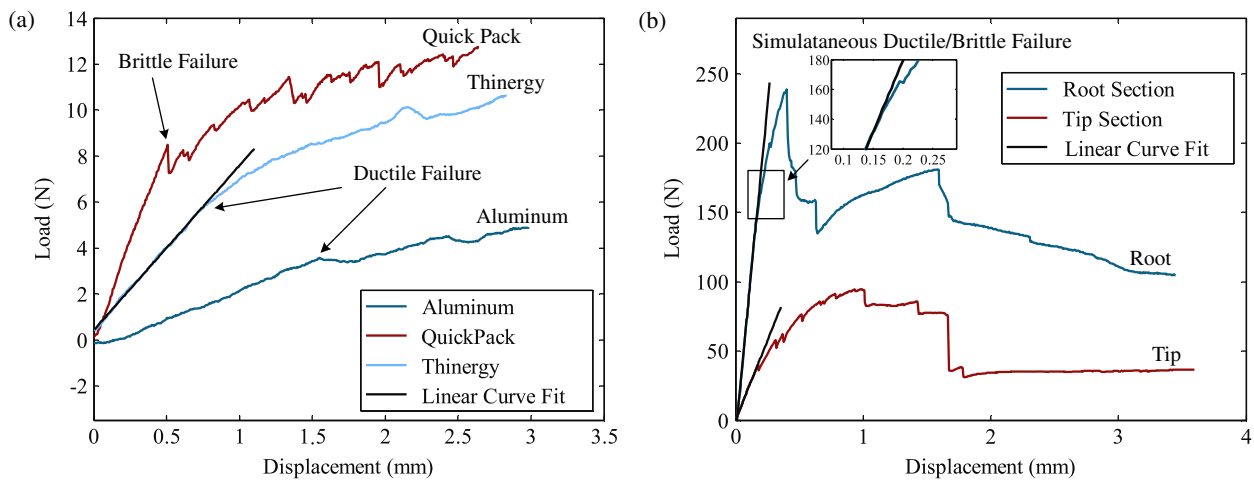


Figure 12. Load-deflection curves for (a) individual layers and (b) complete self-charging structure sections.

Table 3. Failure loads for three-point bending tests.

Parameter	Aluminum substrate	QP10N device	Thinergy® batteries
Failure load (N)	3.21	7.25	6.58
	3.36	8.80	5.47
	3.66	8.50	5.89
Minimum (N)	3.21	7.25	5.47
Complete self-charging structure			
	Root section		Tip section
Failure load (N)	39.9		165.3

Table 4. Maximum stress at failure for three-point bending tests.

Parameter	Aluminum substrate	QP10N Device	Thinergy® batteries
Individual layers			
Failure stress (MPa)	229.27	159.82	199.33
Self-charging structure—root			
Failure stress (MPa)	14.62	99.57	N/A
Self-charging structure—tip			
Failure stress (MPa)	20.15	137.23	155.44

behavior. This phenomenon is likely due to failure occurring in the piezoceramic (brittle) and battery (ductile) layers for nearly the same applied load. The failure load results for all of the specimens tested are presented in table 3.

With the failure loads obtained, equations (12) and (13) can be used to obtain the maximum bending stress values for each sample tested. The minimum failure load value is used in the calculations for the individual layers to give a conservative estimate. For the complete self-charging structure, the overall bending stiffness (\bar{YI}) of the root section (containing only the aluminum substrate and piezoceramic layers) is calculated as $\bar{YI} = 0.0652 \text{ N m}^2$, and of the tip section (containing the

aluminum substrate, piezoceramic layers, and battery layers) is calculated as $\bar{YI} = 0.1960 \text{ N m}^2$. It should be noted that the calculation of failure stress in the QuickPack® piezoceramic layers considers the dimensions of only the active element, ignoring the kapton, as the ceramic experiences brittle failure. The calculated failure strength values for each of the specimens are given in table 4.

From the results, it can be seen that failure in the root section of the self-charging structure is due to failure of the piezoceramic layers. At the point of failure, the maximum stress in the aluminum layer is much less than the failure stress observed in a single aluminum layer. The maximum

stress in the QuickPack[®] is about half of the failure stress obtained for a single layer, however, it is on the same order of magnitude. Although there is a significant difference between the maximum stress of the single layer and composite device, it is typical in brittle failure to observe a wide range of failure loads (thus failure stresses) for a single material. Results for the tip section of the self-charging structure show failure in both the piezoceramic and battery layers with stresses similar to the failure stress of the individual layers in both cases. This result is confirmed by the simultaneous brittle and ductile failure observed in figure 12(b). Overall, it can be concluded that the piezoceramic and battery layers are the critical layers in three-point bending failure.

7.2. Dynamic failure analysis and testing

A series of dynamic strength tests are conducted to gain an understanding of the dynamic loading that can be withstood by the self-charging structures without failure. Using equations (10) and (11), the maximum dynamic stress of the k th layer of a thin self-charging structure under base excitation can be expressed as [24]

$$\sigma_k^f(x_{cr}, t) = -Y_k h_{kn} \frac{\partial^2 w(x, t)}{\partial x^2} \Big|_{x=x_{cr}} + \lambda_k (\bar{e}_{31})_k \frac{v_k(t)}{h_{pk}} \quad (14)$$

where x_{cr} is the critical position on the beam where the curvature is maximum (e.g. it is the root for the fundamental mode of a uniform cantilever), the elastic modulus, Y_k , is the constant electric field modulus for a piezoceramic layer, and $(\bar{e}_{31})_k$, $v_k(t)$, and h_{pk} are the effective piezoelectric constant, voltage output, and thickness of the k th layer if it is a piezoceramic layer. Furthermore $\lambda_k = 1$ if the k th layer is a piezoceramic layer, otherwise it is zero. From equations (10), (11), and (14), the maximum dynamic stress FRF of the k th layer per base acceleration can be obtained as $\sigma_k^f(x_{cr}, t)/\bar{a}_B e^{i\omega t}$. For a given value of base acceleration, the maximum dynamic stress values of the individual layers can be extracted. It is expected that the thin-film batteries may exhibit electrical failure due to harmonic excitation, therefore, the maximum dynamic stress in the battery layer that corresponds to this prescribed electrical failure condition can be called the electrical failure strength of the battery under dynamic loading.

Estimates of the maximum stress-to-base acceleration FRFs of the aluminum, piezoceramic, and battery layers are given in figure 13. The average epoxy thickness between the piezoceramic and aluminum layer is measured as 0.0173 mm whereas the average epoxy layer thickness between the outer kapton and the battery layers is negligible. The distances (h_{kn}) from the neutral axis of the symmetric structure to the outer surfaces of the aluminum, piezoceramic, and battery layers are then estimated as 0.0635 mm, 0.398 mm, and 0.614 mm, respectively. The elastic moduli (Y_k) of these structures are taken as 70 GPa, 69 GPa, and 55 GPa, respectively. Since the aluminum and piezoceramic layers are clamped at the root, the maximum stresses for these layers are expected to be at the root (i.e. $x_{cr} = 0$ in equation (14)), however, since the 25.4 mm long battery layers are located close to the free end of the structure, the maximum stress in the battery layers is expected to be at

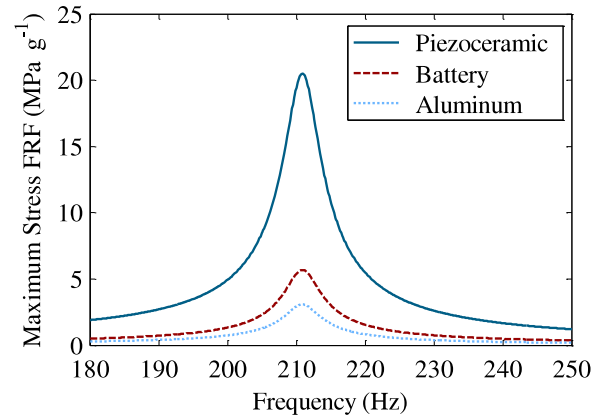


Figure 13. Estimates of the maximum dynamic bending stress in the piezoceramic, battery, and aluminum layers.

the edge of the battery closest to the clamp (which corresponds to $x_{cr} = 18.3$ mm when the device is clamped in the fixture). From the results presented in figure 13, the maximum bending stress per base acceleration of the aluminum, piezoceramic, and battery layers are $5.7 \text{ MPa } g^{-1}$, $20.5 \text{ MPa } g^{-1}$, and $3.1 \text{ MPa } g^{-1}$, respectively. These linear estimates of the stress per base acceleration provide insight into the amount of base acceleration that can be safely imposed on the device. For large-amplitude excitations, however, both geometric and material nonlinearities may exist in the cantilever piezoelectric structure, thus the linear estimates must be used with care.

Dynamic failure testing is conducted using the same experimental setup shown in figure 7 by subjecting the cantilevered harvester to resonant base excitations (previously found to be 210.0 Hz) of increasing amplitude until failure is observed in either the battery layers (electrical failure) or piezoceramic layers (mechanical failure). Electrical failure is defined as a 10% decrease in either the charge or discharge behavior of the battery layers as compared to baseline charge/discharge curves, where mechanical failure is defined as a 10% decrease in the power output of the piezoceramic layers. The self-charging structure is again clamped to the shaker with an overhang length of 43.7 mm and remains undisturbed throughout the duration of the dynamic testing.

An initial baseline charge/discharge measurement is obtained for the device using the power supply (the same procedure used previously to evaluate the performance of the self-charging structures) and all future measurements for battery failure are compared to this baseline. Once the baseline is obtained, the device is first excited at resonance at an initial acceleration input level of $\pm 0.2 g$ for 1 h. During the test, the piezoceramic layers are connected in series to the simple linear regulator harvesting circuit and used to charge a single thin-film battery (which is initially fully discharged to 3.0 V). The battery voltage and current are monitored and recorded in order to evaluate the health of the piezoelectric layers. After 1 h, the excitation is ceased and a discharge test (drawing 2C through a 2749 Ω resistor) is performed on the battery. The self-charging structure is then allowed to sit for 24 h before testing is resumed, as chemical failure in the battery (perhaps due to delaminations) may take time to take

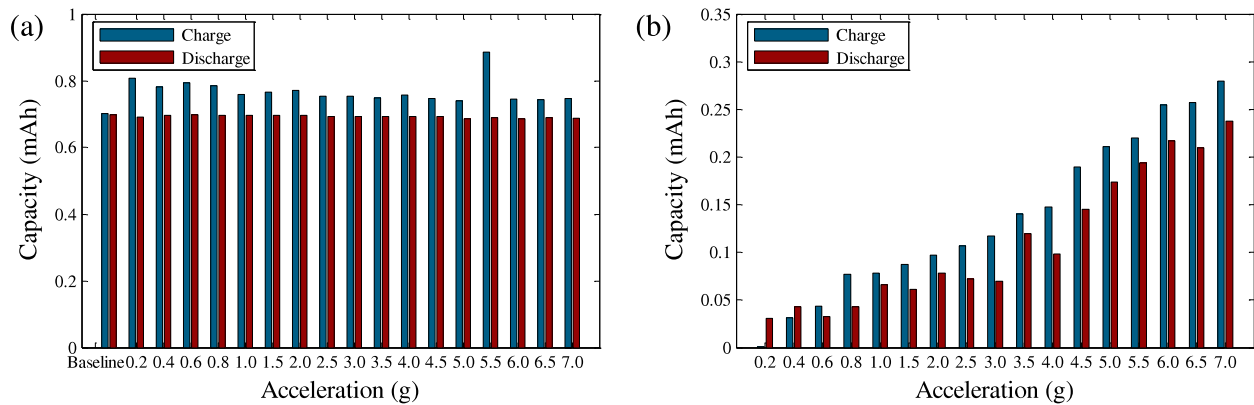


Figure 14. Charge/discharge capacities measured for (a) power supply and (b) piezoceramic charging.

effect. After 24 h, the thin-film battery is charged using the power supply and then discharged. This data is compared to the baseline charge/discharge curves, and significant changes indicate electrical battery failure (caused by the excitation the previous day). Finally, the acceleration amplitude is increased and the process is repeated. It is expected that for larger excitation amplitudes, the piezoelectric layers will provide more power. Deviations in this trend indicate mechanical failure in the piezoelectric layers. Complete results from the dynamic failure testing for the power supply charge/discharge are given in figure 14(a) for base acceleration values from 0.2 g to 7.0 g. Additionally, the charge/discharge results with the piezoceramic layers charging the battery are given in figure 14(b). Based on the maximum stress predictions given in figure 13, an upper limit of 7.0 g (corresponding to 145 MPa of stress in the piezoceramic layer) is chosen. Recall the piezoelectric layer exhibited a maximum stress between 100 and 140 MPa in static failure. Although linear estimates are used here, they provide a reasonable basis for limiting the dynamic excitation level.

From the dynamic failure testing results presented in figure 14(a), it can be seen that as the excitation amplitude is increased from 0.2 g to 7.0 g, there is no significant change in the power supply charge or discharge behavior. In each case, the charge amplitude is slightly higher than the discharge amplitude, likely due to leakage in the battery. The power supply charge after 5.5 g excitation is abnormally high, thus the battery initially appears damaged, but continuation of testing at higher excitation levels shows that the battery still functions properly. This phenomenon may be attributed to experimental variation. Although it was expected that electrical failure would occur in the batteries at the acceleration levels tested, no electrical failure was observed, hence an electrical failure strength cannot be defined for the device.

The piezoceramic charge/discharge results presented in figure 14(b) show that the piezoceramic layers are able to partially charge the thin-film battery. As the excitation amplitude is increased, the total charge capacity (as well as discharge capacity) monotonically increases. This is expected as more vibration energy is available for harvesting at higher excitation levels. The steady increase in charge capacity shows

that no mechanical failure is observed in the piezoelectric layers at the acceleration levels tested. Although a simple linear regulator circuit is used in this study to evaluate the performance of the self-charging structure, more advanced circuitry can be used to improve the amount of energy extracted from the piezoelectric layers and transferred to the battery layers. The authors have previously implemented a nonlinear switching circuit with impedance matching ability and have found that significant increases in efficiency can be obtained for high excitations levels (the power draw of the self-powered switching circuit outweighs any advantages under low level excitation) [29, 6]. The results given in figure 14(b) also show a difference in the charge and discharge capacities for each test. This variability is likely due to leakage in the battery as the current input from the piezoceramic layers is quite low. Overall, the experimental results show that no electrical battery failure or mechanical piezoelectric failure is observed for any of the excitation levels tested.

8. Summary and conclusions

A recent focus has been placed on the development of multifunctional energy harvesting platforms as a method of improving the efficiency of harvesting systems, which can often hinder the operation of their host structures. In this work, multifunctionality is introduced into a piezoelectric energy harvesting system through the combination of energy generation, energy storage, and load bearing ability in a single self-charging structure device. The goal of the self-charging structure concept is to allow direct integration of a piezoelectric energy harvesting device into a host structure in order to provide energy generation and storage ability while minimizing any structural effects caused by the addition of the harvester. This technology is particularly useful in applications where the volume or mass of the host structure is critical.

This paper explores various details of the development and evaluation of the multifunctional self-charging structure concept. Thin-film lithium-based batteries are first evaluated for use in self-charging structures. Thinergy[®] thin-film batteries are found to perform well in both charging and discharging, and are chosen based on their robust construction.

Fabrication of a self-charging structure, consisting of an aluminum substrate, piezoceramic layers, and thin-film battery layers, is then performed. Next, an electromechanical model based on the assumed-modes formulation is employed to describe the coupled behavior of the multifunctional device. Experimental evaluation is performed on the fabricated structure in order to validate the model and confirm the ability of the device to simultaneously harvest and store electrical energy. Results of the vibration testing show that the electromechanical model can successfully predict the voltage output and vibration response of the device under base excitation. Additionally, charge/discharge testing under dynamic excitation verifies the transfer of electrical energy from the piezoceramic layers to the battery layers, thus demonstrating self-charging operation. Lastly, the strength of the self-charging structures is experimentally evaluated both statically and dynamically. Results of static three-point bend testing show that the strength of the composite harvesters is around 100–150 MPa, and that the piezoceramic and battery layers are critical when subject to bending loads. The dynamic strength testing results demonstrate that no electrical or mechanical failure occurs in the device for excitation levels up to 7.0 *g*, proving the self-charging structures to be robust under dynamic excitation.

The results presented in this paper prove the concept of self-charging structures. Simultaneous energy generation and energy storage has been demonstrated in a robust platform capable of supporting structural load. Self-charging structures can be used in various energy harvesting applications where increased functionality can result in an overall improvement in system efficiency.

Acknowledgments

The authors gratefully acknowledge the support of the Air Force Office of Scientific Research MURI under grant no. F9550-06-1-0326 'Energy Harvesting and Storage Systems for Future Air Force Vehicles' monitored by Dr B L Lee. The authors would also like to acknowledge the support of Mac McCord from the Department of Engineering Science and Mechanics at Virginia Tech for help during three-point bend testing, and the support of Na Kong from the Department of Electrical and Computer Engineering at Virginia Tech for help developing energy harvesting circuitry.

References

- [1] Anton S R and Sodano H A 2007 A review of power harvesting using piezoelectric materials (2003-2006) *Smart Mater. Struct.* **16** R1–21
- [2] Cook-Chennault K A, Thambi N and Sastry A M 2008 Powering MEMS portable devices—a review of non-regenerative and regenerative power supply systems with special emphasis on piezoelectric energy harvesting systems *Smart Mater. Struct.* **17** 043001
- [3] Erturk A and Inman D J 2008 A distributed parameter electromechanical model for cantilevered piezoelectric energy harvesters *J. Vib. Acoust.* **130** 041002
- [4] Elvin N G and Elvin A A 2009 A general equivalent circuit model for piezoelectric generators *J. Intell. Mater. Syst. Struct.* **20** 3–9
- [5] Lallart M, Garbuio L, Petit L, Richard C and Guyomar D 2008 Double synchronized switch harvesting (DSSH): a new energy harvesting scheme for efficient energy extraction *IEEE Trans. Ultrason. Ferroelectr. Freq. Control* **55** 2119–30
- [6] Kong N, Ha D S, Erturk A and Inman D J 2009 Resistive impedance matching circuit for piezoelectric energy harvesting *J. Intell. Mater. Syst. Struct.* doi:10.1177/1045389X09357971
- [7] Granstrom J, Feenstra J, Sodano H A and Farinholt K 2007 Energy harvesting from a backpack instrumented with piezoelectric shoulder straps *Smart Mater. Struct.* **16** 1810–20
- [8] Anton S R and Inman D J 2008 Vibration energy harvesting for unmanned aerial vehicles *Proc. 15th SPIE Annual Int. Symp. on Smart Structures and Materials & Nondestructive Evaluation and Health Monitoring (San Diego, CA); Proc. SPIE* **6928** 692824
- [9] Yuse K, Monnier T, Petit L, Lefevre E, Richard C and Guyomar D 2008 Self-powered wireless health monitoring supplied by synchronized switch harvesting (SSH) method *J. Intell. Mater. Syst. Struct.* **19** 387–94
- [10] Christodoulou L and Venables J D 2003 Multifunctional material systems: the first generation *JOM* **55** 39–45
- [11] Thomas J P and Qidwai M A 2004 Mechanical design and performance of composite multifunctional materials *Acta Mater.* **52** 2155–64
- [12] Thomas J P and Qidwai M A 2005 The design and application of multifunctional structure-battery materials systems *JOM* **57** 18–24
- [13] Qidwai M A S, Pogue W R III, Thomas J P and Rohatgi A 2008 Design and fabrication of multifunctional structure-power composites for marine applications *Proc. ASME 2008 Int. Mechanical Engineering Congr. and Exposition (Boston, MA) vol 12, pp 385–93*
- [14] Rohatgi A, Thomas J P, Qidwai M A S and Pogue W R III 2008 Performance characterization of multifunctional structure-battery composites for marine applications *Proc. ASME 2008 Int. Mechanical Engineering Congr. and Exposition (Boston, MA) vol 12, pp 375–83*
- [15] Qidwai M A S, Thomas J P and Pogue W R III 2009 Structure-battery composites for UAVs: multifunctional interaction effects *Proc. 50th AIAA/ASME/ASCE/AHS/ASC Structures, Structural Dynamics, and Materials Conf. (Palm Springs, CA) p AIAA-2009-2341*
- [16] Maung J K, Hahn H T and Ju Y S 2010 Multifunctional integration of thin-film silicon solar cells on carbon-fiber-reinforced epoxy composites *Sol. Energy* **84** 450–8
- [17] Dennler G *et al* 2007 A self-rechargeable and flexible polymer solar battery *Sol. Energy* **81** 947–57
- [18] Kim H S, Kang J S, Park J S, Hahn H T, Jung H C and Joung J W 2009 Inkjet printed electronics for multifunctional composite structure *Compos. Sci. Technol.* **69** 1256–64
- [19] Bates J B, Dudney N J, Gruzalski G R, Zuhr R A, Choudhury A, Luck C F and Robertson J D 1992 Electrical properties of amorphous lithium electrolyte thin films *Solid State Ion.* **1** 53–56 647–54
- [20] Yu X, Bates J B, Jellison G E Jr and Hart F X 1997 Stable thin-film lithium electrolyte: lithium phosphorus oxynitride *J. Electrochem. Soc.* **144** 524–32
- [21] Pereira T, Scaffaro R, Nieh S, Arias J, Guo Z and Thomas Hahn H 2006 The performance of thin-film Li-ion batteries under flexural deflection *J. Micromech. Microeng.* **16** 2714–21

- [22] Pereira T, Scaffaro R, Guo Z, Nieh S, Arias J and Hahn H T 2008 Performance of thin-film lithium energy cells under uniaxial pressure *Adv. Eng. Mater.* **10** 393–9
- [23] Erturk A and Inman D J 2009 An experimentally validated bimorph cantilever model for piezoelectric energy harvesting from base excitations *Smart Mater. Struct.* **18** 025009
- [24] Erturk A, Anton S R and Inman D J 2009 Piezoelectric energy harvesting from multifunctional wing spars for UAVs—part 1: coupled modeling and preliminary analysis *Proc. 16th SPIE Annual Int. Symp. on Smart Structures and Materials & Nondestructive Evaluation and Health Monitoring (San Diego, CA); Proc. SPIE* **7288** 72880C
- [25] du Toit N E and Wardle B L 2007 Experimental verification of models for microfabricated piezoelectric vibration energy harvesters *AIAA J.* **45** 1126–37
- [26] Erturk A 2009 Electromechanical modeling of piezoelectric energy harvesters *PhD Dissertation* Department of Engineering Science and Mechanics Virginia Polytechnic Institute and State University Blacksburg, VA
- [27] Den Hartog J P 1956 *Mechanical Vibrations* (New York: McGraw-Hill)
- [28] Dowling N E 1999 *Mechanical Behavior of Materials: Engineering Methods for Deformation, Fracture, and Fatigue* 2nd edn (Upper Saddle River, NJ: Prentice Hall)
- [29] Anton S R, Erturk A, Kong N, Ha D S and Inman D J 2009 Self-charging structures using piezoceramics and thin-film batteries *Proc. ASME 2009 Conf. on Smart Materials, Adaptive Structures and Intelligent Systems (Oxnard, CA, Sept. 2009)* p SMASIS2009-1368